


Direct Measurement of the  $^{13}\text{C}(\alpha, n)^{16}\text{O}$  Cross Section into the  $s$ -Process Gamow Peak

G. F. Ciani,<sup>1,2,3</sup> L. Cséregi,<sup>1,2,3</sup> D. Rapagnani,<sup>4,5</sup> M. Aliotta,<sup>6</sup> J. Balibrea-Correa,<sup>4,5</sup> F. Barile,<sup>7,8</sup> D. Bemmerer,<sup>9</sup> A. Best,<sup>4,5,\*</sup> A. Boeltzig,<sup>4,5</sup> C. Broggini,<sup>10</sup> C. G. Bruno,<sup>6</sup> A. Cacioli,<sup>10,11</sup> F. Cavanna,<sup>12</sup> T. Chillery,<sup>6</sup> P. Colombetti,<sup>12</sup> P. Corvisiero,<sup>13,14</sup> S. Cristallo,<sup>15,16</sup> T. Davinson,<sup>6</sup> R. Depalo,<sup>11,10</sup> A. Di Leva,<sup>4,5</sup> Z. Elekes,<sup>3</sup> F. Ferraro,<sup>13,14</sup> E. Fiore,<sup>7,8</sup> A. Formicola,<sup>2,†</sup> Zs. Fülöp,<sup>3</sup> G. Gervino,<sup>17,18</sup> A. Guglielmetti,<sup>19,20</sup> C. Gustavino,<sup>21</sup> Gy. Gyürky,<sup>3</sup> G. Imbriani,<sup>4,5</sup> M. Junker,<sup>2</sup> M. Lugaro,<sup>22,23</sup> P. Marigo,<sup>10,11</sup> E. Masha,<sup>19,20</sup> R. Menegazzo,<sup>10</sup> V. Mossa,<sup>8</sup> F. R. Pantaleo,<sup>7,8</sup> V. Patricchio,<sup>8</sup> R. Perrino,<sup>8,‡</sup> D. Piatti,<sup>10,11</sup> P. Prati,<sup>13,14</sup> L. Schiavulli,<sup>7,8</sup> K. Stöckel,<sup>9,24</sup> O. Straniero,<sup>15,2</sup> T. Szücs,<sup>3</sup> M. P. Takács,<sup>9,24</sup> F. Terrasi,<sup>25,5</sup> D. Vescovi,<sup>16,26</sup> and S. Zavatarelli<sup>14</sup>

(LUNA Collaboration)

<sup>1</sup>Gran Sasso Science Institute, Viale F. Crispi 7, 67100 L'Aquila, Italy<sup>2</sup>INFN, Laboratori Nazionali del Gran Sasso (LNGS), 67100 Assergi, Italy<sup>3</sup>Institute for Nuclear Research (ATOMKI), P.O. Box 51, HU-4001 Debrecen, Hungary<sup>4</sup>Università di Napoli "Federico II," 80126 Napoli, Italy<sup>5</sup>INFN, Sezione di Napoli, 80126 Napoli, Italy<sup>6</sup>SUPA, School of Physics and Astronomy, University of Edinburgh, EH9 3FD Edinburgh, United Kingdom<sup>7</sup>Università degli Studi di Bari, 70121 Bari, Italy<sup>8</sup>INFN, Sezione di Bari, 70125 Bari, Italy<sup>9</sup>Helmholtz-Zentrum Dresden-Rossendorf, Bautzner Landstrasse 400, 01328 Dresden, Germany<sup>10</sup>INFN, Sezione di Padova, Via F. Marzolo 8, 35131 Padova, Italy<sup>11</sup>Università degli Studi di Padova, Via F. Marzolo 8, 35131 Padova, Italy<sup>12</sup>INFN, Sezione di Torino, Via Pietro Giuria, 1, 10125 Torino, Italy<sup>13</sup>Università degli Studi di Genova, 16126 Genova, Italy<sup>14</sup>INFN, Sezione di Genova, Via Dodecaneso 33, 16146 Genova, Italy<sup>15</sup>INAF, Osservatorio Astronomico d'Abruzzo, 64100 Teramo, Italy<sup>16</sup>INFN, Sezione of Perugia, Via A. Pascoli snc, 06123 Perugia, Italy<sup>17</sup>Università degli Studi di Torino, 10125 Torino, Italy<sup>18</sup>INFN, Sezione di Torino, Via P. Giuria 1, 10125 Torino, Italy<sup>19</sup>Università degli Studi di Milano, 20133 Milano, Italy<sup>20</sup>INFN, Sezione di Milano, Via G. Celoria 16, 20133 Milano, Italy<sup>21</sup>INFN, Sezione di Roma La Sapienza, Piazzale A. Moro 2, 00185 Roma, Italy<sup>22</sup>Institute of Physics, ELTE Eötvös Loránd University, 1053 Budapest, Hungary<sup>23</sup>Konkoly Observatory, Research Centre for Astronomy and Earth Sciences, MTA Centre for Excellence, 1121 Budapest, Hungary<sup>24</sup>Technische Universität Dresden, Institut für Kern- und Teilchenphysik, Zellescher Weg 19, 01069 Dresden, Germany<sup>25</sup>Università degli Studi della Campania "L. Vanvitelli" (Caserta), 81100 Caserta, Italy<sup>26</sup>Goethe University, Max-von-Laue-Strasse 1, Frankfurt am Main 60438, Germany

 (Received 11 April 2021; revised 8 June 2021; accepted 17 August 2021; published 5 October 2021)

One of the main neutron sources for the astrophysical  $s$  process is the reaction  $^{13}\text{C}(\alpha, n)^{16}\text{O}$ , taking place in thermally pulsing asymptotic giant branch stars at temperatures around 90 MK. To model the nucleosynthesis during this process the reaction cross section needs to be known in the 150–230 keV energy window (Gamow peak). At these sub-Coulomb energies, cross section direct measurements are severely affected by the low event rate, making us rely on input from indirect methods and extrapolations from higher-energy direct data. This leads to an uncertainty in the cross section at the relevant energies too high to reliably constrain the nuclear physics input to  $s$ -process calculations. We present the results from a new deep-underground measurement of  $^{13}\text{C}(\alpha, n)^{16}\text{O}$ , covering the energy range 230–300 keV, with drastically reduced uncertainties over previous measurements and for the first time providing data directly inside the  $s$ -process Gamow peak. Selected stellar models have been computed to estimate the impact of our revised reaction rate. For stars of nearly solar composition, we find sizeable variations of some isotopes, whose production is influenced by the activation of close-by branching points that are sensitive to the neutron density, in particular, the two radioactive nuclei  $^{60}\text{Fe}$  and  $^{205}\text{Pb}$ , as well as  $^{152}\text{Gd}$ .

DOI: 10.1103/PhysRevLett.127.152701

Low-mass asymptotic giant branch (AGB) stars are major production sites of heavy elements in the Universe (for a recent review, see [1]). Their interior contains a carbon-oxygen core surrounded by a thin He-rich mantel and a H-rich envelope. Periodically, these stars undergo thermonuclear instabilities, He-burning flashes, called thermal pulses (TPs). Each He flash generates a large convective zone that mixes the C produced by the triple- $\alpha$  reaction up to the top of the He mantel. Later on, the shell-H burning, always active at the base of the envelope, dies down and, in turn, the external convection penetrates the He-rich mantel. This phenomenon, which moves the nucleosynthesis yields up to the stellar surface, is called the “third dredge up.” As early recognized, the creation of a  $^{13}\text{C}$  pocket within the He-rich mantel, through the reaction  $^{12}\text{C}(p,\gamma)^{13}\text{N}(\beta^+)^{13}\text{C}$ , is a by-product of these recursive mixing episodes [2,3]. Such a thin pocket (a few  $10^{-5}M_{\odot}$  of  $^{13}\text{C}$ ) harbors one of the most important nucleosynthesis sites in the Universe. During the period between two TPs, the temperature attains about 90 MK and  $^{13}\text{C}$  is activated as a neutron source through the reaction  $^{13}\text{C}(\alpha,n)^{16}\text{O}$ . This process provides a relatively slow neutron flux [ $\approx 10^7$  neutrons/(s cm $^2$ )] for about  $10^4$  years each time. Starting from seed nuclei in the iron region, this neutron flux slowly builds up heavy elements along the line of stability [4]. This  $s$  process (“slow neutron capture”) is responsible for the production of about half of all the heavy elements ( $A \geq 90$ ) in the Universe.

In order to constrain this important nucleosynthesis process, the cross section of the  $^{13}\text{C}(\alpha,n)^{16}\text{O}$  neutron source needs to be known in the astrophysical energy window (the Gamow peak) around  $E_0 = 150\text{--}230$  keV [5]. The available direct cross-sectional data in the lower-energy interval  $280 < E < 350$  keV [6,7] are affected by uncertainties  $\geq 40\%$ . Any effort of pushing direct reaction measurements to lower energies is basically rendered futile by the steep drop of the cross section and the presence of natural and instrumental backgrounds. Extrapolation of the cross section into the Gamow peak is further complicated by a broad state at  $E_x = 6356(8)$  keV ( $J^{\pi} = \frac{1}{2}^+$ ) just near the  $\alpha$  threshold in  $^{17}\text{O}$  ( $S_{\alpha} = 6359$  keV [8]). The cross section evaluation in the Gamow peak requires a careful matching between the tail of this near-threshold state and the higher-energy experimental data. While this state has been the focus of great experimental attention over the past years [9–13], its influence remains a major source of uncertainty for the  $s$  process [14] and the need for more cross-sectional data to fill the gap has been frequently expressed [14,15].

In order to provide direct data at low energies to better constrain the cross section inside the Gamow peak, the LUNA Collaboration has performed an intensive experimental campaign at the deep-underground accelerator LUNA400 [16] inside the Gran Sasso National Laboratory (LNGS). The LNGS neutron background flux

( $\approx 10^{-7}$  n cm $^2$  s) [17] is dominated by the natural radioactivity of the surrounding rock and it is up to 4 orders of magnitude lower than on the surface of Earth, improving the sensitivity over previous studies.

The experimental setup and the target analysis are described in detail in Refs. [18–20], and the following is a brief summary. The accelerator provided a  $\text{He}^+$  beam on target of up to  $150 \mu\text{A}$  with  $\alpha$  energies of 305–400 keV, corresponding to c.m. energies in the range 233–306 keV. Deposited charges vary from 15 C at the highest to 90 C at the lowest energy. The beam impinged upon water-cooled targets made of an 99% enriched  $^{13}\text{C}$  evaporated on a 0.2 mm thick Ta backing [18].

Near the target, the beam passed a liquid-nitrogen-cooled shroud and an electrically insulated collimator at a negative voltage of 300 V (to suppress the effects of secondary electrons). The neutrons produced by the  $^{13}\text{C}(\alpha,n)^{16}\text{O}$  reaction, with energies around 2.4 MeV, were thermalized in a polyethylene moderator and detected by 18  $^3\text{He}$ -filled proportional counters with stainless steel housing. Two geometrical detector configurations (a vertical and a horizontal orientation) were used to optimize the absolute neutron detection efficiency,  $34 \pm 3\%$  and  $38 \pm 3\%$ , respectively [19]. Moreover, the measurement reproducibility was checked by separately analyzing datasets acquired with the two detector configurations at the same energy, finding agreement in the final results. The detector signals were digitized with a 100 MHz sampling rate and analyzed off-line to suppress the internal background from  $\alpha$  decays in the steel housing of the counters using a custom pulse-shape discrimination (PSD) technique [21]. The PSD in combination with the borated polyethylene shielding (5 and 10 in., depending on the setup) around the detector, as well as the underground location results in a total background rate inside the neutron signal region of  $1.2 \pm 0.1$  counts/h for both configurations, leading to an improvement by more than 2 orders of magnitude compared with previous experiments.

Blank backings were irradiated obtaining a background level of  $1.3 \pm 0.2$  counts/h, in agreement with the environmental one. The conclusion was that the beam-induced background was negligible. The evaporated  $^{13}\text{C}$  targets were characterized in terms of homogeneity and thickness immediately after the evaporation at ATOMKI by means of the  $^{13}\text{C}(p,\gamma)^{14}\text{N}$  resonance at  $E_{r,\text{lab}} = 1748$  keV. The average target thickness at resonance energy was 5 keV, corresponding to 170 nm. Because of the cross-sectional reduction of one order of magnitude, the differential neutron yield becomes negligible from reactions occurring beyond 150 nm inside the target, so all the targets can be considered to be of the same effective thickness. At LUNA, target quality was frequently checked (every 1.5 C accumulated charge) using direct  $\gamma$ -ray measurements of the  $^{13}\text{C}(p,\gamma)^{14}\text{N}$  reaction [18].

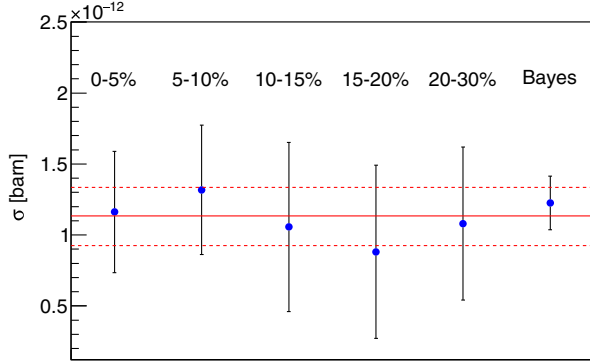


FIG. 1. Comparison of the cross section at 233 keV for different target degradation and the Bayesian results. The solid and dashed lines represent the weighted average of the groups and the corresponding uncertainty, respectively.

The cross section was calculated as follows:

$$Y = \frac{\eta(E_\alpha)}{Qe} \int_{E_\alpha - \Delta E}^{E_\alpha} \frac{\sigma(E)}{\epsilon_{\text{eff}}(E)} dE, \quad (1)$$

where  $Y$  is the number of detected neutrons per projectile (PSD corrected),  $\eta$  is the neutron detection efficiency,  $Qe$  is the incident number of particles on the target,  $E_\alpha$  is the beam energy,  $\epsilon_{\text{eff}}(E)$  is the effective stopping power, and  $\Delta E$  is the projectile energy loss in the target.

The maximum accumulated  $\alpha$  charge on each target was limited to 3 C, corresponding to at most a 30% degradation. The lowest energies  $E = 245$  and  $E = 233$  keV required special attention, as the statistics collected during a single run was insufficient to obtain a reliable estimate of the cross section. Two independent approaches were used in the analysis. In the first one, all runs at the same energy with similar target degradation levels were summed together and the cross sections for each “subset” were calculated and combined to the cross section for this energy. In the second one, the two lowest energies were also analyzed using a Bayesian approach [22]; see the Supplemental Material for details [23].

In Fig. 1, the 233 keV cross sections as a function of target degradation are compared with the Bayesian results. The mean values are in agreement; the “grouping” method was used for the extraction of the cross sections presented later in this Letter.

The experimental results are summarized in Table I, where we also show the  $S$  factor [24] after correcting for the electron screening effect [25] (bare in Table I), following Refs. [26–28]. The Table includes statistical and systematic uncertainties. The latter are 3% for the charge integration, 5% for stopping power calculated with SRIM-2010 [29], and about 8% for the detection efficiency. The uncertainty of the beam energy is around 300 eV, and the beam energy spread is less than 100 eV [16].

The new data extend the energy range covered by direct cross-sectional measurements into the  $s$ -process Gamow

TABLE I. Experimental and electron screening-corrected  $S$  factors. The data format is  $\text{data} \pm \text{stat} \pm \text{syst}$ , where  $\text{syst}$  is a common systematic uncertainty of 10% (further details in the text).

Energy (keV)	$S$ factor ( $10^5$ MeV b)	$S$ factor ( $10^5$ MeV b) (bare)
306	$8.06 \pm 0.18 \pm 0.8$	$7.61 \pm 0.17 \pm 0.8$
298	$8.1 \pm 0.3 \pm 0.8$	$7.6 \pm 0.3 \pm 0.8$
291	$7.3 \pm 0.3 \pm 0.7$	$6.8 \pm 0.3 \pm 0.7$
283	$8.6 \pm 0.3 \pm 0.9$	$8.0 \pm 0.3 \pm 0.8$
275	$9.2 \pm 0.6 \pm 0.9$	$8.6 \pm 0.5 \pm 0.9$
260	$8.7 \pm 0.8 \pm 0.9$	$8.1 \pm 0.7 \pm 0.8$
245	$11.7 \pm 1.7 \pm 1.2$	$10.8 \pm 1.5 \pm 1.1$
233	$12.7 \pm 2.3 \pm 1.3$	$11.6 \pm 2.1 \pm 1.2$

peak, but an extrapolation toward zero energy, also taking into account the near-threshold state ( $E_x = 6356$  keV,  $J^\pi = \frac{1}{2}^+$ ), is still required. This was done with an  $R$ -matrix analysis using the code *Azure2* [30]. The low-energy cross section is dominated by two broad states, the already mentioned near-threshold state and a  $\frac{3}{2}^+$ ,  $E_x = 7215$  keV one. Narrow resonances in the energy range covered by the analysis ( $E < 1.2$  MeV) do only have very localized effects on the cross sections and were omitted. As the threshold state was assumed to be  $\alpha$  bound, an asymptotic normalization coefficient instead of an  $\alpha$  partial width was used [11]. Energy and width or asymptotic normalization constant (ANC) of the threshold state were kept fixed (note that they were varied in the Monte Carlo analysis, see below). Channel radii of 4.15 and 6.684 fm were used for the neutron and  $\alpha$  channels, respectively. In addition to the cross sections from Heil *et al.* and Drotleff *et al.*, the data by Harissopoulos *et al.* [31] were included in the analysis, as they cover a wider energy range and help better constrain the  $\approx 800$  keV resonance. A normalization factor of 1.37 was applied to the latter to match the absolute scales of the different datasets. Two high-energy poles were included to take into account the influence of higher-lying resonances on the cross section. Their widths and that of the  $E_x = 7215$  keV state were kept free. The parameters resulting from the  $R$ -matrix fit are given in Table II. The top panel of Fig. 2 shows the experimental  $S$  factors and the  $R$ -matrix

TABLE II.  $R$ -matrix parameters and datasets.

$E_x$ (keV)	$\Gamma_n$ (keV)	$\Gamma_\alpha   \text{ANC}$ (keV)   (fm $^{-1/2}$ )	Dataset	Normalization
6356	124	$5.44 \times 10^{90}$	Drotleff <i>et al.</i> [6]	1
7215	305.3	$9.75 \times 10^{-2}$	Heil <i>et al.</i> [7]	1
15 000	$2.42 \times 10^4$	$6.04 \times 10^5$	Harissopoulos <i>et al.</i> [31]	1.37
15 000	$4.33 \times 10^2$	$6.02 \times 10^5$	This Letter	1

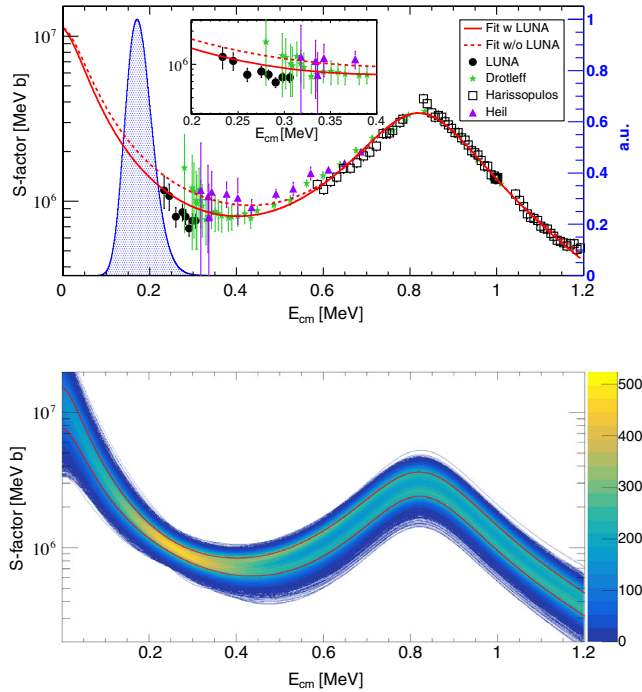


FIG. 2. Top: astrophysical  $S$  factor of  $^{13}\text{C}(\alpha, n)^{16}\text{O}$ . The lines show the results of two  $R$ -matrix analyses, with and without the new data. The Harissopulos dataset was normalized according to value in Table II. The blue curve is the “Gamow peak” at 90 MK and the right y axis refers to its relative scale. Bottom: Monte Carlo probability density for the  $S$  factor.

fits with (solid line) and without (dashed line) our new LUNA data.

The uncertainties in the final cross section were investigated using a Monte Carlo (MC) approach. The ANC and the neutron partial width of the threshold state, as well as the absolute scales of the four experimental datasets, were randomly sampled from a Gaussian distribution according to their respective uncertainties. To be conservative, a 12% uncertainty was assumed for the absolute scale of each dataset. 30 000 MC variations were evaluated and the  $R$ -matrix cross sections of each run were saved for later processing. The density map of the results and traditional  $1\sigma$  contours are displayed in Fig. 2. As mentioned above, the cross sections from [31] are rescaled to match the data of [6,7], as in other recent papers. However, there are no strong motivations for doing so, and one could choose to instead base the normalization on the Harissopulos *et al.* data (as suggested by a recent measurement [32]). To investigate the effect of the two different normalizations, we performed  $R$ -matrix calculation using data by Harissopulos *et al.* as a reference for the normalization of [6,7]. Inside the Gamow peak, the effect is only of the order of 5%, increasing toward higher energies. The absolute scale of the normalization of the historical data is still a matter for debate. Therefore, in the MC procedure, only for the sake of the determination of a lower limit, we

also considered the case (for half of the total trials) of using unscaled Harissopulos *et al.* [31] data, while the [6,7] normalizations were changed accordingly. It is worth noting that this additional source of uncertainty contributes only marginally, about 5%, at the  $s$ -process energies, where the cross section is well constrained by the present data, while it has a larger impact at higher energies [33]. As will be discussed below, the establishment of a reliable lower limit is crucial for the determination of possible nucleosynthesis variations. In total, three different rates were calculated: LUNA, using the  $R$ -matrix best fit including the new cross sections; no-LUNA, the best fit without the new data; and low-LUNA using the fifth percentile of the fit adopting the Harissopulos normalization. The no-LUNA and low-LUNA cover approximately the  $\pm 95\%$  percentiles around the best fit.

Finally, the astrophysical reaction rate  $R = N_A \langle \sigma v \rangle$  as a function of stellar temperature was calculated (in units of  $\text{cm}^3 \text{mol}^{-1} \text{s}^{-1}$ ) by integration of the  $R$ -matrix cross section,

$$R = \frac{3.7318}{T_9^{3/2}} \sqrt{\frac{M_0 + M_1}{M_0 M_1}} \times \int_0^\infty E \sigma(E) e^{-11.605E/T_9} dE, \quad (2)$$

where  $T_9$  is the temperature in gigakelvin, the energy is given in MeV, the cross section  $\sigma$  in barn, and the  $M_i$  are the atomic masses of the reaction partners. Probability density functions for the rate were generated based on the results of the various MC cross sections. The contributions from the narrow resonances were, as usual, summed to the final rate. Tabulated results are shown in the Supplemental Material accompanying this Letter [23].

In the  $s$  process in AGB stars [3,35], shortly after a third-dredge-up episode, a  $^{13}\text{C}$  pocket forms within the He-rich mantle. During the following interpulse period, this region heats up and, around  $\sim 80$ – $100$  MK, the  $^{13}\text{C}(\alpha, n)^{16}\text{O}$  reaction starts to release neutrons. The high neutron exposure ( $\sim 0.4 \text{ mb}^{-1}$  in solar metallicity stars) coupled to a low neutron density (a few  $10^6 \text{ n/cm}^3$ ) are the two major features of the resulting  $s$ -process nucleosynthesis. The first ensures a neutron flux over a time long enough to produce a large overabundance of all the elements belonging to the main component of the  $s$  process ( $A > 90$ ), while the second favors  $\beta^-$  decays over neutron captures at the various branching points of the  $s$ -process path. In most cases, the  $^{13}\text{C}$  pocket is fully consumed during the interpulse period. However, if a small amount of  $^{13}\text{C}$  survives (i.e., if the reaction rate is low enough), it will be engulfed into the convective shell powered by the subsequent thermal pulse and burned at a higher temperature ( $\sim 200$  MK) [36]. This second (convective) neutron burst is characterized by a higher neutron density ( $> 10^9 \text{ n/cm}^3$ ), but much lower neutron exposure, than the main (radiative) event. As a consequence, it does not modify the bulk of stellar yields, but may affect some key



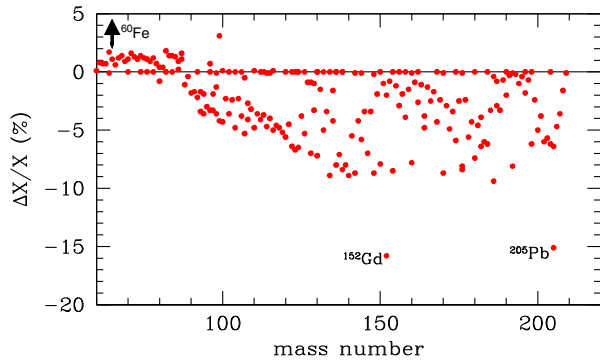


FIG. 3. Percentage variations of the mass fractions of heavy isotopes in the low-LUNA model with respect to the no-LUNA model. In both models, the final surface composition is the cumulative result of 11 third-dredge-up episodes. The  $^{60}\text{Fe}$  variation (+102%) is out of the scale and marked by an arrow.

isotopes at the  $s$ -process branching points [37]. Extant models of low-mass AGB stars have shown that this second neutron burst may occur during the first few thermal pulses, in stars with metallicity  $Z \geq 0.01$  and that its efficiency is sensitive to the adopted  $^{13}\text{C}(\alpha, n)^{16}\text{O}$  reaction rate [15].

In order to evaluate the impact of the new reaction rate on the  $s$  process, we have calculated three models of an AGB star with mass  $M = 2M_{\odot}$ , metallicity  $Z = 0.02$ , and  $Y = 0.27$ , under the three different assumptions (LUNA and the  $\sim \pm 95\%$  values corresponding to no-LUNA and low-LUNA) for the  $^{13}\text{C}(\alpha, n)^{16}\text{O}$  rate mentioned above. In all the three models, some  $^{13}\text{C}$  survives at the end of the first two interpulse periods and is burned at high temperature in the convective thermal pulse. Stronger effects of this second neutron burst are expected for the low-LUNA case. The results are compared in Fig. 3. More details on the stellar models are given in the Supplemental Material [23], which includes Refs. [38–40].

Most of the nuclei belonging to the main component are depressed when the  $^{13}\text{C}(\alpha, n)^{16}\text{O}$  rate is lowered. This is the natural consequence of the suppression of the radiative  $s$  process. The reduction of the surface abundances is stronger for the heavier isotopes ( $A > 130$ ). The heavy- $s$  (Ba, La, Ce, Nd, Sm) to light- $s$  (Sr, Y, Zr) abundance ratio is an important spectroscopic index, often used to probe the mean neutrons to seeds ratio of an  $s$ -process site [41]. At the end of the AGB phase, the (heavy- $s$ /light- $s$ ) ratio of the low-LUNA model is  $\sim 6\%$  smaller than in the no-LUNA model. The abundance variations are generally small ( $\leq 10\%$ ), with interesting exceptions, i.e.,  $^{60}\text{Fe}$ ,  $^{152}\text{Gd}$ , and  $^{205}\text{Pb}$ . All these isotopes are sensitive to the neutron density because of the existence of close-by branching points.  $^{152}\text{Gd}$  cannot be produced by the  $r$ -process and, except for a small  $p$ -process contribution, is mainly synthesized by the  $s$  process. On the other hand,  $^{60}\text{Fe}$  and  $^{205}\text{Pb}$  are short-lived radioactive isotopes that were found to be alive in the early Solar System [42]. The  $^{60}\text{Fe}$  is

produced when the neutron density is high enough to allow neutron captures at the  $^{59}\text{Fe}$  branching point (half-life 44.5 d). Therefore, its final abundance is enhanced in case of the activation of the second (convective) neutron burst. With respect to the no-LUNA model, we find that the  $^{60}\text{Fe}$  final mass fraction is 30% higher in the LUNA model and a factor of 2 higher in the low-LUNA model. On the contrary, the production of both  $^{152}\text{Gd}$  and  $^{205}\text{Pb}$  requires low neutron density, while they are mainly destroyed in case of high neutron density. Indeed, the first isotope is bypassed by the  $s$  process when the  $^{151}\text{Sm}$  may capture a neutron before decaying into  $^{151}\text{Eu}$ . Similarly, the  $^{205}\text{Pb}$  production is suppressed when the  $^{204}\text{Tl}$  branch is open. Therefore, their production is reduced when the  $^{13}\text{C}(\alpha, n)^{16}\text{O}$  rate is lowered, as it happens for all the other isotopes of the main component, and a further decrease of their abundances occurs in case of a more efficient second (convective) neutron burst. As a result, the final mass fractions of both isotopes are reduced by 15% at the 95% lower bound.

To conclude, the present Letter reports a much improved calculation of the  $^{13}\text{C}(\alpha, n)^{16}\text{O}$  reaction rate at  $T \sim 90$  MK, for the first time based on direct data inside of the Gamow window. The reduced uncertainty will help our understanding of the  $s$ -process branching points that are sensitive to the neutron density. We find that the new low-energy cross-sectional measurements imply sizeable variations of the  $^{60}\text{Fe}$ ,  $^{152}\text{Gd}$ , and  $^{205}\text{Pb}$  yields. Other isotopes, whose production or destruction are influenced by close-by branching points, such as the two neutron-magic nuclei  $^{86}\text{Kr}$  and  $^{87}\text{Rb}$  as well as  $^{96}\text{Zr}$ , are less affected by a variation of the  $^{13}\text{C}(\alpha, n)^{16}\text{O}$  reaction rate, mainly because of their higher initial (solar) abundance. However, we cannot exclude that larger changes may occur in models with different initial mass and composition. For this reason, a more extended set of AGB models is required to accurately evaluate the general impact on the galactic chemical evolution.

This work has been supported by the INFN. D. Ciccotti of the LNGS and proved to be invaluable over the course of the campaign. We acknowledge the support of the mechanical workshops of INFN-LNGS and INFN-Na. Financial support is acknowledged as follows. D. V., the German-Israeli Foundation (GIF No. I-1500-303.7/2019); A. Be, A. Bo, A. D. L., G. I., and D. R. received funding from the European Research Council (ERC No. 852016); A. Be. and J. B.-C., the University of Naples-Compagnia di San Paolo Grant No. STAR-2016; L. Cs., T. S., Zs F., Gy. G., the Hungarian National Research Development and Innovation Office NKFIH (Contracts No. PD129060, No. K120666, and No. K134197); T. S., the Jnos Bolyai Research Fellowship of the Hungarian Academy of Sciences and NKP-20-5-DE-297 New National Excellence Program of the Ministry of Human Capacities of Hungary; D. B., DFG (BE 4100/4-1); M. A., C. G. B., T. C., T. D., STFC-UK.

R. D. and D. P. acknowledge funding from the Italian Ministry of Education, University and Research (MIUR) through the Dipartimenti di eccellenza project Science of the Universe. A. Be. is grateful to Richard J. deBoer for discussions about the  $R$ -matrix analysis.

\*Corresponding author.  
andreas.best@unina.it

†Corresponding author.  
formicola@lngs.infn.it

‡Permanent address: INFN Sezione di Lecce, Via Arnesano, 73100 Lecce, Italy.

- [1] C. Sneden, J. J. Cowan, and R. Gallino, *Annu. Rev. Astron. Astrophys.* **46**, 241 (2008).
- [2] O. Straniero, R. Gallino, and S. Cristallo, *Nucl. Phys. A* **777**, 311 (2006).
- [3] R. Gallino, C. Arlandini, M. Busso, M. Lugaro, C. Travaglio, O. Straniero, A. Chieffi, and M. Limongi, *Astrophys. J.* **497**, 388 (1998).
- [4] F. Käppeler, R. Gallino, S. Bisterzo, and W. Aoki, *Rev. Mod. Phys.* **83**, 157 (2011).
- [5] All energies in this Letter are center-of-mass energies, unless explicitly stated otherwise.
- [6] H. W. Drotleff, A. Denker, H. Knee, M. Soine, G. Wolf, J. W. Hammer, U. Greife, C. Rolfs, and H. P. Trautvetter, *Astrophys. J.* **414**, 735 (1993).
- [7] M. Heil, R. Detwiler, R. E. Azuma, A. Couture, J. Daly, J. Görres, F. Käppeler, R. Reifarh, P. Tischhauser, C. Ugalde *et al.*, *Phys. Rev. C* **78**, 025803 (2008).
- [8] D. R. Tilley, H. R. Weller, and C. M. Cheves, *Nucl. Phys. A* **564**, 1 (1993).
- [9] S. Kubono, K. Abe, S. Kato, T. Teranishi, M. Kurokawa, X. Liu, N. Imai, K. Kumagai, P. Strasser, M. H. Tanaka *et al.*, *Phys. Rev. Lett.* **90**, 062501 (2003).
- [10] E. D. Johnson, G. V. Rogachev, A. M. Mukhamedzhanov, L. T. Baby, S. Brown, W. T. Cluff, A. M. Crisp, E. Diffenderfer, V. Z. Goldberg, B. W. Green *et al.*, *Phys. Rev. Lett.* **97**, 192701 (2006).
- [11] M. L. Avila, G. V. Rogachev, E. Koshchiy, L. T. Baby, J. Belarge, K. W. Kemper, A. N. Kuchera, and D. Santiago-Gonzalez, *Phys. Rev. C* **91**, 048801 (2015).
- [12] O. Trippella and M. L. Cognata, *Astrophys. J.* **837**, 41 (2017).
- [13] N. Keeley, K. W. Kemper, and K. Rusek, *Eur. Phys. J. A* **54**, 71 (2018).
- [14] R. J. deBoer, C. R. Brune, M. Febraro, J. Görres, I. J. Thompson, and M. Wiescher, *Phys. Rev. C* **101**, 045802 (2020).
- [15] S. Cristallo, M. L. Cognata, C. Massimi, A. Best, S. Palmerini, O. Straniero, O. Trippella, M. Busso, G. F. Ciani, F. Mingrone *et al.*, *Astrophys. J.* **859**, 105 (2018).
- [16] A. Formicola, G. Imbriani, M. Junker, D. Bemmerer, R. Bonetti, C. Brogгинi, C. Casella, P. Corvisiero, H. Costantini, G. Gervino *et al.*, *Nucl. Instrum. Methods Phys. Res., Sect. A* **507**, 609 (2003).
- [17] A. Best, J. Görres, M. Junker, K.-L. Kratz, M. Laubenstein, A. Long, S. Nisi, K. Smith, and M. Wiescher, *Nucl. Instrum. Methods Phys. Res., Sect. A* **812**, 1 (2016).
- [18] G. F. Ciani, L. Csedreki, J. Balibrea-Correa, A. Best, M. Aliotta, F. Barile, D. Bemmerer, A. Boeltzig, C. Brogгинi, C. G. Bruno *et al.*, *Eur. Phys. J. A* **56**, 75 (2020).
- [19] L. Csedreki, G. Ciani, J. Balibrea-Correa, A. Best, M. Aliotta, F. Barile, D. Bemmerer, A. Boeltzig, C. Brogгинi, C. Bruno *et al.*, *Nucl. Instrum. Methods Phys. Res., Sect. A* **994**, 165081 (2021).
- [20] G. F. Ciani, Ph.D. thesis, Gran Sasso Science Institute and SISSA, 2019.
- [21] J. Balibrea-Correa, G. Ciani, R. Buompane, F. Cavanna, L. Csedreki, R. Depalo, F. Ferraro, and A. Best, *Nucl. Instrum. Methods Phys. Res., Sect. A* **906**, 103 (2018).
- [22] A. Caldwell, D. Kollár, and K. Kröninger, *Comput. Phys. Commun.* **180**, 2197 (2009).
- [23] See Supplemental Material at <http://link.aps.org/supplemental/10.1103/PhysRevLett.127.152701> for tabulated reaction rates, information about the two lowest energy data points and more details on target degradation treatment and the stellar models.
- [24] The astrophysical  $S$  factor is defined as  $\sigma(E) = S(E)(1/E)e^{-2\pi\eta}$  and is commonly used to remove the strong energy dependence in the cross section due to the Coulomb repulsion.  $\eta = 0.1575Z_a Z_b \sqrt{(1/E)[M_a M_b / (M_a + M_b)]}$  is the Sommerfeld parameter.
- [25] A screening potential of 937 V was used for the calculations: the corresponding correction is less than 10% for all the energies.
- [26] F. Strieder, B. Limata, A. Formicola, G. Imbriani, M. Junker, D. Bemmerer, A. Best, C. Brogгинi, A. Caciolli, P. Corvisiero *et al.*, *Phys. Lett. B* **707**, 60 (2012).
- [27] L. Bracci, G. Fiorentini, V. Melezhik, G. Mezzorani, and P. Quarati, *Nucl. Phys. A* **513**, 316 (1990).
- [28] K.-N. Huang, M. Aoyagi, M. H. Chen, B. Crasemann, and H. Mark, *At. Data Nucl. Data Tables* **18**, 243 (1976).
- [29] J. F. Ziegler, M. Ziegler, and J. Biersack, *Nucl. Instrum. Methods Phys. Res., Sect. B* **268**, 1818 (2010).
- [30] R. E. Azuma, E. Uberseder, E. C. Simpson, C. R. Brune, H. Costantini, R. J. de Boer, J. Görres, M. Heil, P. J. LeBlanc, C. Ugalde, and M. Wiescher, *Phys. Rev. C* **81**, 045805 (2010).
- [31] S. Harissopulos, H. W. Becker, J. W. Hammer, A. Lagoyannis, C. Rolfs, and F. Strieder, *Phys. Rev. C* **72**, 062801(R) (2005).
- [32] M. Febraro, R. J. deBoer, S. D. Pain, R. Toomey, F. D. Becchetti, A. Boeltzig, Y. Chen, K. A. Chipps, M. Couder, K. L. Jones *et al.*, *Phys. Rev. Lett.* **125**, 062501 (2020).
- [33] New measurements of the higher-energy cross section are planned at various facilities worldwide, including with the upcoming LUNA MV accelerator at the LNGS [34], addressing this uncertainty.
- [34] F. Ferraro, G. F. Ciani, A. Boeltzig, F. Cavanna, and S. Zavatarelli, *Front. Astron. Space Sci.* **7**, 119 (2021).
- [35] O. Straniero, R. Gallino, M. Busso, A. Chieffi, C. M. Raiteri, M. Limongi, and M. Salaris, *Astrophys. J.* **440**, L85 (1995).
- [36] S. Cristallo, O. Straniero, R. Gallino, L. Piersanti, I. Domínguez, and M. T. Lederer, *Astrophys. J.* **696**, 797 (2009).
- [37] S. Bisterzo, R. Gallino, F. Käppeler, M. Wiescher, G. Imbriani, O. Straniero, S. Cristallo, J. Görres, and R. J. deBoer, *Mon. Not. R. Astron. Soc.* **449**, 506 (2015).

- [38] S. Cristallo, L. Piersanti, O. Straniero, R. Gallino, I. Domínguez, C. Abia, G. Di Rico, M. Quintini, and S. Bisterzo, *Astrophys. J. Suppl. Ser.* **197**, 17 (2011).
- [39] D. Vescovi, S. Cristallo, M. Busso, and N. Liu, *Astrophys. J. Lett.* **897**, L25 (2020).
- [40] A. I. Karakas and M. Lugaro, *Astrophys. J.* **825**, 26 (2016).
- [41] M. Busso, R. Gallino, and G. J. Wasserburg, *Annu. Rev. Astron. Astrophys.* **37**, 239 (1999).
- [42] G. J. Wasserburg, M. Busso, R. Gallino, and K. M. Nollett, *Nucl. Phys.* **A777**, 5 (2006).